Journal of Colloid and Interface Science 615 (2022) 227–235

Contents lists available at ScienceDirect

Journal of Colloid and Interface Science

journal homepage: www.elsevier.com/locate/jcis

Droplet splashing on curved substrates

Thomas C. Sykes [a,*], Ben D. Fudge [a], Miguel A. Quetzeri-Santiago [b], J. Rafael Castrejón-Pita [c], Alfonso A. Castrejón-Pita [a,*]

[a] Department of Engineering Science, University of Oxford, Oxford OX1 3PJ, United Kingdom
[b] Mesoscale Chemical Systems Group, MESA+ Institute and Faculty of Science and Technology, University of Twente, Enschede 7500AE, The Netherlands
[c] School of Engineering and Materials Science, Queen Mary University of London, London E1 4NS, United Kingdom

GRAPHICAL ABSTRACT

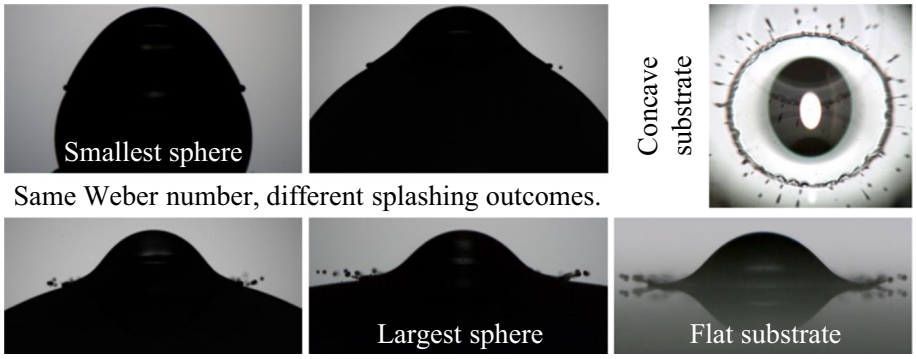

ARTICLE INFO

Article history:
Received 2 November 2021
Revised 20 January 2022
Accepted 21 January 2022
Available online 29 January 2022

Keywords:
Droplets
Splashing
Textured substrates
Wetting
Droplet impact

ABSTRACT

Droplets impacting dry solid substrates often splash above a certain threshold impact velocity. We *hypothesise* that substrate curvature alters splashing thresholds due to a modification to the lift force acting on the lamella at the point of breakup. We have undertaken high-speed imaging *experiments* of millimetric droplets impacting convex and concave surfaces to establish splashing thresholds and dynamics across a wide range of substrate geometries and impact conditions. Our *findings* indicate that the tendency of droplets to splash is proportional to the reciprocal of the substrate's radius of curvature, independent of whether the substrate is convex or concave, with it being harder for droplets to splash on small spheres. Moreover, we consistently parameterise the axisymmetric splashing threshold across all curved substrate geometries via a modification to the well-known splashing ratio. Finally, the splashing dynamics resulting from initial asymmetry between the impacting droplet and curved substrate are also elucidated.

1. Introduction

Droplet impact onto solid substrates arises throughout industry and nature, which has motivated extensive work on the topic since the seminal work of Worthington in the 19th century [1]. Despite the resulting body of literature, droplet impact is still captivating scientists for its wide range of outcomes, from simple spreading

* Corresponding authors.
E-mail addresses: thomas.sykes@eng.ox.ac.uk, t.c.sykes@outlook.com (T.C. Sykes), castrejon@cantab.net (J.R. Castrejón-Pita), alfonso.castrejon-pita@wadham.ox.ac.uk (A.A. Castrejón-Pita).

https://doi.org/10.1016/j.jcis.2022.01.136
0021-9797/

and deposition to bouncing and splashing (i.e. droplet fragmentation) [2,3]. The parameters governing the physics of impact, including droplet properties, substrate characteristics (including wettability and temperature), and the ambient pressure, are broad and intricately linked, with many playing pivotal roles in the resulting dynamics [4–11]. Droplet impact phenomena have been traditionally characterised via the Weber, $We = \rho u^2 l/\sigma$, and Reynolds, $Re = \rho u l/\mu$, numbers, where μ, σ, ρ, u, and l are the droplet's dynamic viscosity, surface tension, density, impact velocity, and a characteristic length scale (typically the droplet diameter), respectively. In this context, simple deposition typically occurs at low Weber and Reynolds numbers. In contrast, at sufficiently high Weber and Reynolds numbers, an impacting droplet splashes, breaking-up into secondary droplets (satellites).

Understanding the conditions under which splashing occurs is of utmost importance in applications including spray processes, forensic science, and inkjet printing [3]. In many cases, research and development aims to prevent fluid misting and the formation of smaller droplets with indiscriminate trajectories, both of which can affect finish quality and aerosolise potentially-hazardous fluids [12]. Whilst past works have mainly focused on droplets impacting flat surfaces, some natural and industrial applications see droplets impacting concave or convex substrates instead, including individual spherical particles. Examples of these processes include spray drying, rain-induced icing, and the inkjet printing of a binder on powder beds for additive manufacturing [13,14]. Notably, inkjet printing applications are seeking to expand into textured surface markets, such as in the food industry, aerospace, and automotive.

Past works have demonstrated that droplets impacting a dry spherical target can produce at least seven distinct outcomes: deposition, rebound, coating, gravity disintegration, momentum disintegration, and splashing [13,15–17]. These outcomes are dependent on the impact velocity, liquid properties, substrate wettability, surface roughness (as for flat substrates [18]), and the sphere size relative to the droplet diameter. Most droplet impact studies on spheres have been conducted at moderate Weber numbers ($We < 100$), finding larger wetting areas on spherical substrates than on flat ones, for similar impact conditions [19–21]. Similarly, it has been shown that increasing substrate curvature (i.e. smaller spheres) leads to droplets spreading to a larger maximum spreading diameter, while also enhancing receding following maximum spreading [22,23]. In contrast, few studies have been conducted under the parameter range leading to splashing [e.g. 24–26], despite its practical significance [13]. Other studies have been focused on wet surfaces, which strongly influences impact outcomes [e.g. 27,28]. In fact, some of these works present contradictory results regarding the influence of the substrate curvature on splashing thresholds.

In this work, we study the effect of substrate curvature on the propensity of an impacting droplet to splash using high-speed imaging. Our experimental conditions cover a wide range of parameters, encompassing simple deposition through to corona splashing. Our experimental protocol (involving two high-speed cameras positioned perpendicularly to determine impact position) enables the transition between simple deposition and splashing to be precisely delineated across a range of curved substrates, including convex spheres (covering an order-of-magnitude wide range of diameters), a flat substrate, and concave surfaces. Moreover, by considering the effect of substrate curvature on the lift force acting on the lamella at the onset of splashing, we identify a potential mechanism underpinning the splashing threshold and propose a modification to the well-known splashing ratio [5,29] to account for the effect of substrate curvature.

2. Experimental method

Single ethanol droplets (density, $\rho = 785\ \mathrm{kg\ m^{-3}}$; surface tension, $\sigma = 22.2\ \mathrm{mN\ m^{-1}}$; dynamic viscosity, $\mu = 1.10\ \mathrm{mPa\ s}$ [30]) were impacted onto smooth untreated borosilicate-glass substrates. Ethanol strongly wets untreated glass, with a static contact angle of $(5 \pm 4)^\circ$, and a quasistatic advancing contact angle of $(20 \pm 3)^\circ$ [10,18]. These angles were measured using a polynomial fitting approach, as detailed in Ref. [31] (also see Fig. 1d). The contact line usually pinned at the maximum spread length, if achieved; the receding contact angle is close to 0°, implying a contact angle hysteresis of approximately 20°. Characterised by their apex radius of curvature, r_s, the substrates were eight convex spheres (Bearing Warehouse Ltd and Glass Sphere s.r.o.), covering an order-of-magnitude wide range of $r_s \in [2.0, 20.0]$ mm, two plano-concave lenses with $r_s \in \{-25.84, -12.92\}$ mm (KPC040 and KPC043, Newport), and a flat cover slip ($r_s \to \infty$). All substrates were thoroughly cleaned and dried between successive impacts.

Droplets were generated by dripping from a blunt-end dispensing tip (Metcal or Fisnar) at 15 μL $\mathrm{min^{-1}}$ using a syringe pump, until the pendant droplet detached due to gravity and fell vertically towards the substrate. Two dispensing tip sizes (22 and 25 gauge) were used interchangeably to adjust droplet volume; the distance between the dispensing tip and substrate apex was varied (180 mm–400 mm) to adjust the impact velocity, $u \in [1.77, 2.58]\ \mathrm{m\ s^{-1}}$, as measured using an in-house MATLAB script. Impact velocities were selected to comprehensively span the splashing threshold of each substrate. As noted by other authors for millimetric droplets generated by dripping (e.g. Ref. [32]), oscillations in the free surface of the falling droplets meant that they were not necessarily spherical on impact, whilst it is known that droplet shape influences splashing [33]. These oscillations were accounted for by measuring the radius of curvature of the bottom of the droplet, r_c at the point of impact (see the solid part of the droplet's edge in Fig. 1a). We take $l = 2r_c$ as the characteristic length scale to approximate the effective diameter of the droplet for the purposes of splashing (e.g. $We = \rho u^2 \cdot 2r_c/\sigma$). For a typical experiment (oblate droplet), r_c was generally 5% greater than the equivalent spherical radius, with variations in r_c around 4% for a fixed droplet volume – see §1 of the Supplemental Material for details. In this work, $We \in [237, 539]$, $Re \in [2544, 4221]$, and $Oh = \sqrt{We}/Re = \mu/\sqrt{\rho\sigma l} \in [5.3 \times 10^{-3}, 6.1 \times 10^{-3}]$.

The dispensing tips and substrates were attached to manual translation and elevation stages, providing each with independent 3-axis motion, enabling the impact position to be varied and axisymmetry between the droplet and substrate to be ensured when desired. All impacts were simultaneously imaged using two high-speed cameras positioned perpendicularly, in a shadowgraphy setup. For the convex substrates, both cameras were focused on the apex of the sphere, as seen in Fig. 1b (not to scale; similarly for the flat substrate). One camera, either a Phantom TMX 7510 or v2512 recording at 25,000–110,000 frames per second (fps), was principally used to image the droplet geometry and impact dynamics with an 105–199 pixels $\mathrm{mm^{-1}}$ effective resolution. The second camera, either a Phantom v12.1 or Miro LAB310 recording at up to 11,000 fps, with 34–99 pixels $\mathrm{mm^{-1}}$, gave a wider view of the dynamics. The two cameras together enabled the impact point in the horizontal plane of a top-down view to be precisely determined. Further technical details of the experiment are provided in §2 of the Supplemental Material. Also described there is a modified setup used for the concave surfaces, where the higher-speed camera imaged the splashing dynamics through the bottom of the substrate via a mirror.

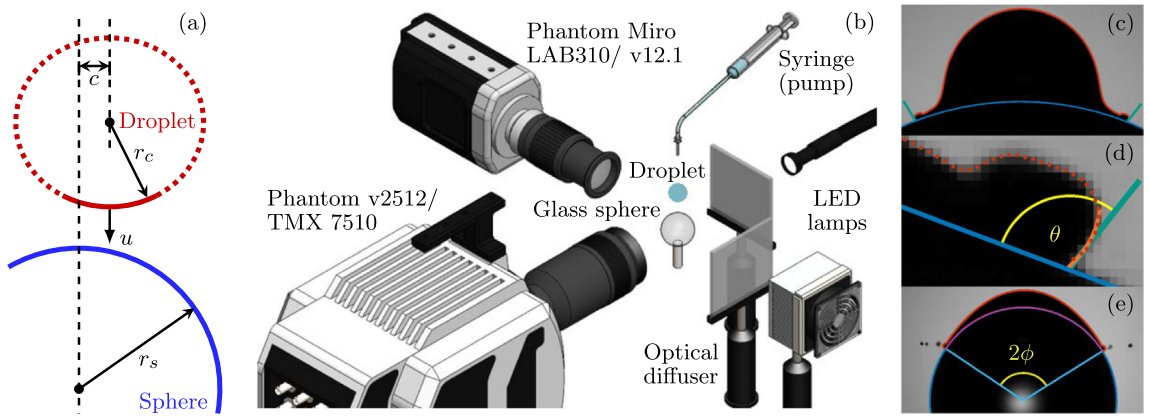

Fig. 1. (a) A sketch of droplet impact onto a convex substrate (sphere), labelled with pertinent geometric variables and impact velocity. c refers to the radial offset in a 2D horizontal plane of the substrate and droplet's vertical axes of symmetry; zero offset out of the plane of the figure is assumed here. Axisymmetric impact implies that $c \approx 0$, as in Sections 3.1 and 3.2. (b) A sketch of the accompanying experimental setup. (c)–(e) Image-processed frames: red points represent detected edge pixels; orange line indicates the fitted polynomial; green lines are tangent to the free surface at the contact point.

For convex substrates, the dynamic contact angle, θ was measured for all times $t > 0$ ($t = 0$ on impact) using a polynomial fitting approach, as seen in Figs. 1c and 1d [31]. The orange line in Fig. 1d represents the fitted polynomial; the green line represents the tangent to the polynomial at the contact point, from which θ is measured relative to the tangent to the sphere's surface. The angle subtended by the radial lines to the contact points at the centre of the sphere, 2ϕ and the spread length (purple line) were also measured – see Fig. 1e.

3. Results and discussion

3.1. Splashing propensity and dynamics

For fixed $We = 414 \pm 2$ ($Re = 3533 \pm 35; K = We^{1/2}Re^{1/4} = 157 \pm 1$), Fig. 2 (and the accompanying videos) demonstrates that the splashing propensity of a $(3.79 \pm 0.08)\mu L$ droplet impacting a sphere axisymmetrically depends strongly on substrate curvature, r_s. Note that τ represents dimensionless time ($\tau = 0$ on impact), with respect to the kinetic time scale, $2r_c/u$. Within our experiments, both prompt and corona splashing is seen. Solely for the classification of droplet impact outcomes, no distinction is made between prompt and corona splashing; any break-up of the droplet during the outward spreading phase is considered splashing[1]. Splashing is therefore seen for all $r_s \geqslant 3.0$ mm in Fig. 2, whilst the droplet simply spreads across the $r_s = 2.0$ mm sphere. The $r_s \in \{3.0, 4.0\}$ mm spheres show splashing behaviour akin to prompt splashing, whilst more comprehensive corona-like breakup is evident for $r_s \in \{7.0, 20.0\}$ mm. Indeed, corona splashing is known to occur for such impact conditions on smooth flat glass substrates (as seen in the bottom row of Fig. 2), which is far from the splashing threshold, just above which prompt splashing ensues. Hence, Fig. 2 substantiates the qualitative conclusion that it is harder for impacting droplets to splash on smaller spheres. Moreover, Fig. 2 qualitatively demonstrates that satellite trajectories, number and volume distributions vary on curved substrates for fixed impact conditions, further indicating the significant affect of substrate curvature on post-splashing dynamics that could be of interest in natural and industrial contexts, as previously elucidated for flat targets [35,36]. A detailed study of such post-splashing dynamics represents an excellent opportunity to extend this work.

[1] There are other mechanisms of secondary droplet formation, such as induced by a droplet spreading into a convex substrate's mount or over the rim of a concave substrate (as recently demonstrated by Ref. [34]) and gravity disintegration; these mechanisms are not considered as splashing here.

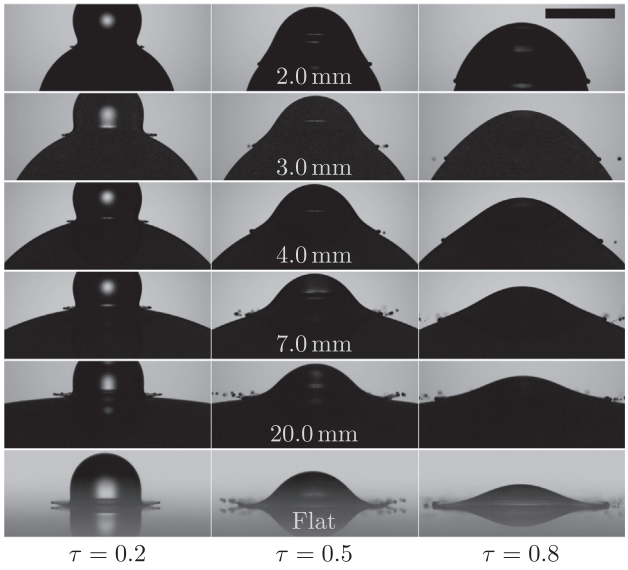

Fig. 2. Axisymmetric impact of fixed-volume ethanol droplets onto a selection of convex substrates, and a flat glass side (bottom row), at constant $We = 414 \pm 2$. Substrate curvature, r_s, is indicated in the centre of each row. Times τ are dimensionless with respect to the kinetic time scale, $2r_c/u$. Normalised offset $c/r_c \ll 0.1$. The scale bar is 2 mm.

For a quantitative assessment of splashing thresholds, the splashing propensity of $(3.6 \pm 0.3)\mu L$ droplets are presented as a regime map in Fig. 3a, in terms of the traditional splashing parameter $K = We^{5/8}Oh^{-1/4} = We^{1/2}Re^{1/4}$, and the ratio of droplet to substrate curvature $\Omega = r_c/r_s$. The latter enables comparison to existing studies [28,26]. Defining c as the dimensional horizontal radial offset of the substrate and droplet's vertical axes of symmetry on impact (see Fig. 1a, where zero offset out of the plane of the figure is assumed), only $\Omega > 0$ experiments with $c/r_c < 0.15$ are plotted to ensure axisymmetry (cf. Section 3.3). The splashing threshold region for each substrate is defined as $K \in [K_l, K_h]$, where $K_l = \min(K) \forall K$ showing splashing, and $K_h = \max(K) \forall K$ not exhibiting splashing. Individual experiments are plotted as separate points and coloured according to splashing outcome. Those points outside the threshold region are faded, with the vertical extent of the threshold region commensurate to the error in determining K. $K \approx 127$ (black-dashed line in Fig. 3a) is the accepted splashing threshold for ethanol droplets impacting flat dry sub-

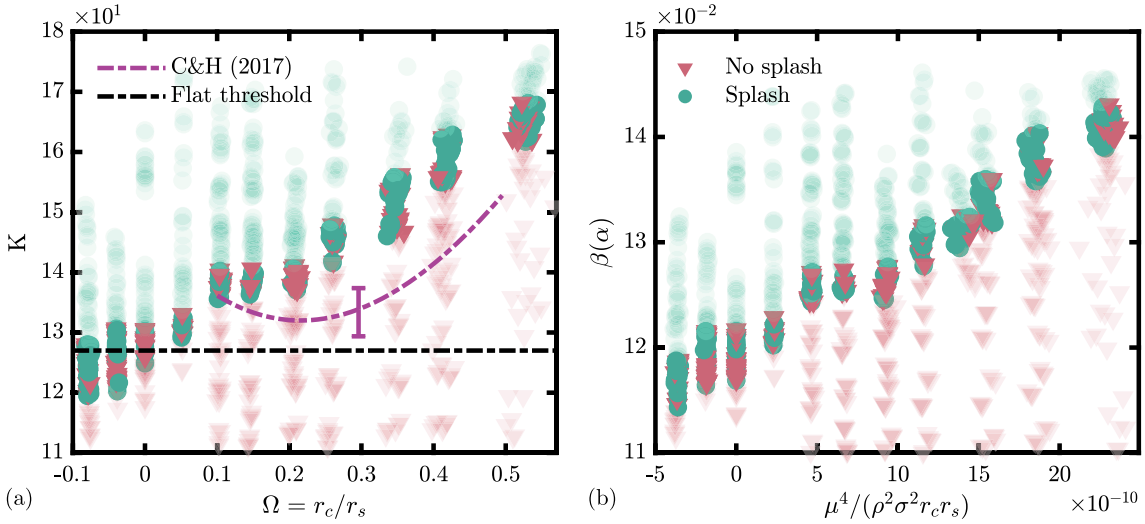

Fig. 3. Splashing propensity of (3.6 ± 0.3)μL droplets (originating from a 25 gauge dispensing tip) impacting convex ($r_s > 0$), concave ($r_s < 0$), and flat ($r_s \to \infty$) substrates, in terms of the splashing parameter $\mathrm{K} = \mathrm{We}^{5/8}\mathrm{Oh}^{-1/4}$ and splashing ratio $\beta(\alpha)$. (4.85 ± 0.15)μL droplet data are also included in panel (b). All impacts are axisymmetric ($c/r_c < 0.15$ for $r_s > 0$ data). 'C&H (2017)' refers to the polynominal fit found in Ref. [26] for micrometric droplets with $\Omega \in [0.09, 0.55]$. The flat threshold of $\mathrm{K} \approx 127$ is sourced from Refs. [37,10], which is consisten.t with our data.

strates (i.e. $r_s \to \infty$ and $\Omega = 0$) [37,10], which is consistent with our data.

$\Omega > 0$ for spheres, whilst $\Omega < 0$ for concave surfaces. Examples of impact dynamics on both concave substrates studied are seen in Fig. 4. In the first three rows, $\mathrm{We} \in [302, 337]$ is varied on the $r_s = -12.92$ mm substrate. Interestingly, there are a similar number of satellite droplets for the two $\mathrm{We} \in \{314, 337\}$ cases exhibiting splashing. Due to the satellite's shallower trajectory, more land back on the substrate for the $\mathrm{We} = 314$ example (seen as long streaks in the $\tau = 0.6$ frames). We did not observe satellites landing on spheres of similar $|\, r_s \,|$ values: concave surfaces curve upwards to intersect the satellites' trajectories. Satellites that land within the maximum spread length of the primary droplet are able to recoalesce with it (see $\tau = 0.9$), which is significant from the point of view of applications wishing to avoid contamination resulting from splashing [12]. For fixed $\mathrm{We} = 337$ (bottom two rows of Fig. 4), more satellites materialise on the substrate with greater $|\, 1/r_s \,|$ (i.e. $r_s = -12.92$ mm, 3rd row of Fig. 4), and also appear to have a greater volume (with a greater potential for secondary breakup). These qualitative observations indicate that the trend in splashing propensity on spheres identified above continues into concave surfaces, which is quantitatively confirmed in Fig. 3a. Note that the $\Omega < 0$ data shown in Fig. 3a have been filtered according to the axisymmetry condition $c/r_c < 0.15$. However, there is additional uncertainty in the apex position relative to the droplet location on impact here. Nevertheless, the splashing dynamics are well separated and consistent for both concave examples.

Fig. 3a shows unique behaviour in comparison to the existing literature. Charalampous and Hardalupas (2017), herein 'C&H (2017)', considered the impact of micrometric droplets (diameter $[170, 280]$μm) onto dry spheres of three different diameters ($\{500, 1000, 2000\}$μm), with droplets continuously impinging at up to 20000 Hz [26]. The splashing threshold was found to be $\mathrm{We} \approx 400$ for $0.09 < \Omega < 0.30$, and increased to $\mathrm{We} \approx 450$ for $\Omega \approx 0.5$. Their polynomial fit describing the splashing threshold (extracted from figure 12 of C&H (2017), in terms of We) is plotted in terms of K with our data in Fig. 3a. Ω values are taken directly from the source, assuming that $\mathrm{Oh} = 8 \times 10^{-3}$; the error bar represents uncertainty in $\mathrm{Oh} \in [7.0 \times 10^{-3}, 8.9 \times 10^{-3}]$. The trend broadly agrees with our data for $\Omega > 0.3$, being only one or two

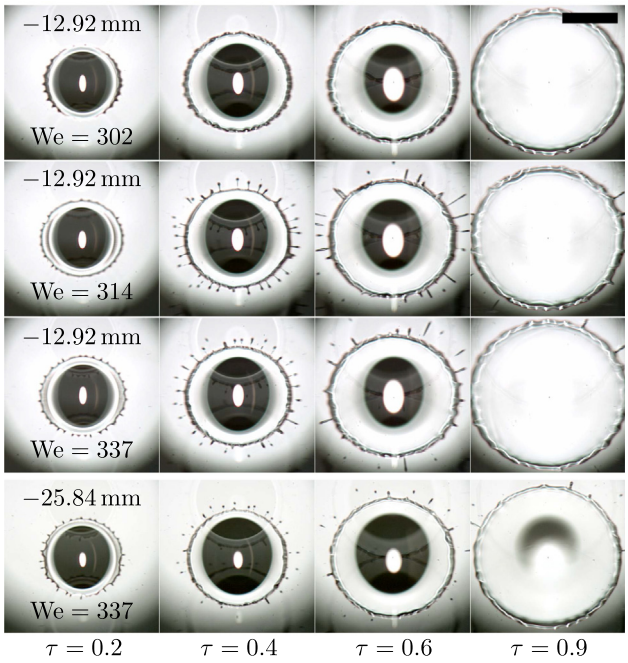

Fig. 4. Axisymmetric impact of ethanol droplets onto a selection of concave surfaces, viewed from below (through the substrate). Substrate curvature, r_s is indicated in each row, along with We. Times τ are dimensionless with respect to the kinetic time scale, $2r_c/u$. Note that droplets appear ellipsoidal in these images due to a slight misalignment between the mirror and curved target (concave lens). The scale bar is 2 mm.

standard deviations away, but diverges after a minimum at $\Omega < 0.3$. C&H (2017) noted that their observations disagreed with a 1999 paper that considered impact onto dry spheres (but still with continuous impingement at 1000 Hz), which concluded that it was easier to splash on small spheres [25]. A qualitatively-similar trend was obtained by Liang et al. (2014) for impact onto wetted spheres (with a pre-existing film of varying thickness: 12 μm–61 μm). The splashing threshold of millimetric heptane droplets ($\mathrm{Oh} = 2.6 \times 10^{-3}$, diameter 1.8 mm) on spheres was found to approximately coincide with that of a flat substrate for

$\Omega < 0.224 : \mathrm{We} = 124$, corresponding to $\mathrm{K} = 90$ [28]. Indeed, the presence of a thin film is known to reduce the splashing threshold of heptane droplets on smooth flat substrates [38]. In Liang et al.'s work, for smaller spheres ($\Omega > 0.224$), the splashing threshold increased approximately linearly with Ω, similar to our data. Their observed $\Omega < 0.224$ behaviour may owe to the pre-existing thin film, which could decrease the effective substrate curvature and alter the lift force acting on the lamella (see Section 3.2). With the benefit of a wider range of $\Omega \in [-0.08, 0.55]$, a thoroughly-dry substrate, and verifiable-axisymmetry, our work demonstrates that the splashing threshold on dry curved substrates consistently increases with increasing Ω over concave, flat, and convex substrates.

For a single liquid and a unique flat substrate, K is sufficient to parameterise splashing thresholds, though they are also affected by the surrounding gas pressure [39] (amongst other factors), which K does not account for. In recent times, for smooth flat hydrophobic substrates, low-Oh splashing has been successfully parameterised by a splashing ratio

$$\beta(\alpha) = \frac{2.22}{\tan\alpha}\frac{\mu_g^{1/2}(\rho r_c u^5)^{1/6}}{\sigma^{2/3}}, \tag{1}$$

which was derived assuming that splashing results from the growth of capillary instabilities as aerodynamic forces (the sum of gas lubrication and suction forces) lift the advancing lamella off the substrate [5,40,29,41]. Here, $\mu_g = 1.8 \times 10^{-5}$ Pa s is the gas' dynamic viscosity, r_c is the chosen length scale, and α is the *wedge angle* between the substrate and lamella at the onset of splashing. $\alpha \approx 60^\circ$ for smooth flat substrates, independent of wettability [41]. Splashing on smooth flat substrates, from wetting to superhydrophobic, has been successfully parameterised using $\beta(\alpha)$ and the dynamic contact angle [10]. The theory underpinning $\beta(\alpha)$ has also been extended to rough substrates [42], and to explain splashing suppression of micron-sized droplets [43].

Accordingly, our experimental data is plotted in terms of $\beta(\alpha)$ in Fig. 3b. The flat threshold ($r_s \to \infty$) of $\beta(\alpha) \approx 0.12$ is consistent with existing data for hydrophilic flat substrates: Ref. [41] reports a splashing threshold of 0.120 ± 0.008 for ethanol–water mixtures, taking the radius as the length scale. For spheres, increasing either r_c or r_s promotes splashing, whilst they have opposite effects on Ω. Hence, we plot against the dimensionless quantity $\mu^4/(\rho^2\sigma^2 r_c r_s)$ instead in Fig. 3b, which is Oh^4 with $l = \sqrt{r_c r_s}$, the geometric mean of the radii of curvature, so $\mathrm{Oh}^4 \propto 1/(r_c r_s)$. Our larger droplet volume ($(4.85 \pm 0.15)\mu$L) data, for $r_s = 3.0$ mm, are also plotted in Fig. 3b, whose threshold is seen to be consistent with the existing $(3.6 \pm 0.3)\mu$L data, which would not be the case if plotting against Ω.

3.2. Splashing mechanism

We now wish to explain the trend in splashing propensity seen in Fig. 3 from a physical perspective. Our hypothesis is that the propensity to splash decreases as $1/r_s$ increases due to a modification to the lift force on the lamella, which can be accounted for geometrically. For a general geometry, we define an effective wedge angle α^*, where $\alpha^* = \psi + \phi$. In Fig. 5a, ψ is the angle between the tangent to the lamella at the contact point and the horizontal, whilst ϕ is the angle between the horizontal and downstream tangent to the substrate at the contact point (if $r_s < 0$, then $\phi < 0$), both at the onset of breakup. Herein, all angles are reported in radians.

Whilst $\phi = 0$ for a flat substrate (with $\alpha = \psi = \pi/3$), ϕ is non-zero for curved substrates. Geometrically, ϕ is also the angle subtended by the substrate between the vertical axis and contact point, at the centre of the substrate's curvature (see Fig. 5a). Therefore, $s = r_s\phi$, where s is half of the spread length of the droplet along the curved substrate at the onset of breakup. Note that $\phi \to 0$ as $r_s \to \infty$, as required for a flat substrate. Fig. 5b presents s measured for a selection of our experiments, plotted against $1/r_s$; error bars represent the variation between different experiments. The data shows that s, within experimental error, does not depend on the substrate curvature. A similar conclusion was reached in C&H (2017) with micrometric droplets; their data, extracted from figure 16, is also plotted in Fig. 5b (green points, plotted against Ω). Hence, $s = 1.9$ mm, delineated by the dashed line in Fig. 5b, is taken as a fixed constant value, within experimental error for all curvatures in Fig. 5b. Consequently, ϕ can be regraded as a geometric property of the substrate.

The angle between the tangent to the lamella at the contact point and the horizontal at the onset of breakup, ψ would be expected to decrease as $1/r_s$ increases, since the surrounding gas is easier to drain from beneath the lamella on smaller spheres. This variable was measured for a selection of our splashing experiments, noting that $\psi = \pi - \theta - \phi$ (see Figs. 1d and 5a), and plotted in Fig. 5c against $1/r_s$, alongside equivalent data from C&H (2017), extracted from figure 17 (green points, plotted against Ω); the error bars represent variation between different experiments. We note here the appreciable challenges of both accurately determining the exact time of breakup and measuring the true dynamic contact angle for splashing studies in general [41,10,44]; hence, the relatively large experimental uncertainty in ψ. Moreover, for convex substrates, if any part of the lamella falls below the horizontal plane containing the contact point (always if $\psi \lesssim 0$; often the case for small $\psi > 0$), then the true contact point (and therefore θ) is hidden by the revolved lamella. See the darker lamella region of the sketch inset in Fig. 5a, where the hidden contact point is indicated. In such cases, θ and ψ cannot be measured from an external side view (as in this work). Despite these challenges, Fig. 5c indicates that ψ varies linearly with respect to $1/r_s$. Note that ψ, an offset contact angle, should not depend on r_c, given that contact angles are determined by the chemical properties of the substrate and wetting fluid [45,46]. Recalling that $\psi = \pi/3$ at $1/r_s = 0$ (flat substrate), the linear dependence on r_s implies that $\psi = \pi/3 + m/r_s$ for a gradient m.

The effective wedge angle on curved substrates, α^* is therefore given by

$$\alpha^* = \psi + \phi = \frac{\pi}{3} + \frac{m+s}{r_s}. \tag{2}$$

Recall from Section 3.1 that $\beta(\alpha) \approx 0.12$ (flat substrates). Moreover, $s = 1.9$ mm is constant, which suggests that $m = -1.75$ mm to parameterise the effect of substrate curvature. This value of m indicated by the slope of the triangle in Fig. 5c, which is consistent (within identified errors) with both data sets shown. Hence, the data in Fig. 3b are replotted with the splashing ratio corrected for substrate curvature by substituting Eqn. (2) into Eqn. (1) with $m + s = 0.15$ mm, denoted $\beta(\alpha^*)$, in Fig. 6. As seen, $\beta(\alpha^*) \approx 0.12$ for all concave, convex, and flat substrates studied. That is, $\beta(\alpha^*)$ yields a consistent splashing threshold for axisymmetric impact, regardless of substrate curvature.

Substrate curvature can therefore be taken into account in Eqn. (1) using the effective wedge angle α^*. Note that the origin of the constant wedge angle for flat substrates is the relative position of the contact point and the tip of the lamella, due to the no-slip condition [40]. On spheres, the contact point moves downwards by a constant amount for a given curvature (given that s is fixed), effectively opening the gap between the lamella and substrate, notwithstanding the relative ease of draining gas from beneath the lamella. The relative change in the vertical position of the contact point depends on the size of the sphere, showing that α^* depends on r_s. In other words, $\alpha^* > \pi/3$ characterises the effective increase in

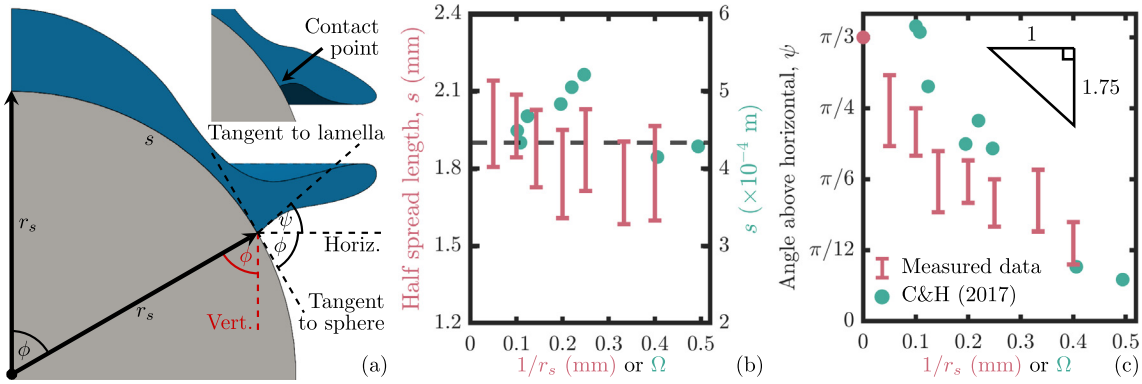

Fig. 5. (a) Sketch of a droplet spreading on a sphere, at the point of lamella breakup, with variables pertinent to the proposed mechanism indicated. Not to scale. Note that $\alpha^* = \phi + \psi$. The inset sketch shows that the contact point in a 2D vertical plane (indicated) can be hidden by the 3D revolved lamella (darker blue) from an external view. (b) Half spread length on the curved substrate at the onset of breakup, s, against a measure of substrate curvature. The dashed line indicates the constant value of $s = 1.9$ mm. (c) ψ (at the onset of breakup) against the same measure of substrate curvature. For both graphs, axis labels are colour-coded according to relevant data; red data was measured from our convex substrate experiments that splash; green data was extracted from C&H (2017) [26]. Error bars represent variation between differ.ent experiments.

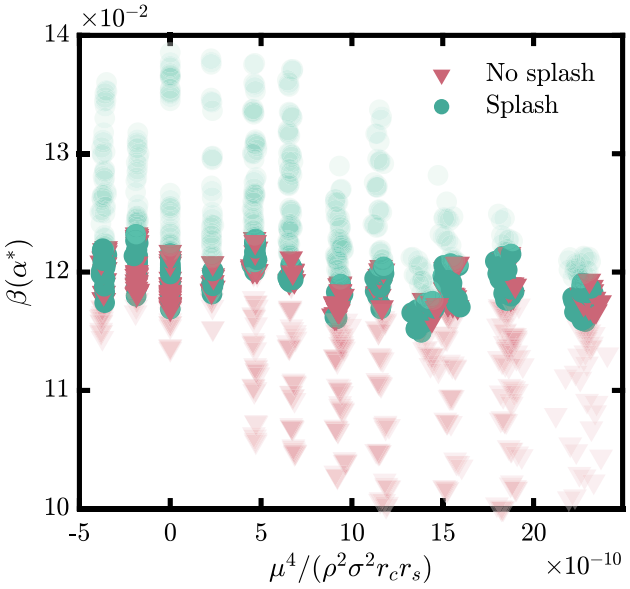

Fig. 6. Splashing propensity of (3.6 ± 0.3)μL and (4.85 ± 0.15)μL droplets parameterised by the splashing ratio corrected for substrate curvature using the wedge angle given in (2), denoted $\beta(\alpha^*)$, with $s = 1.9$ mm and $m = -1.75$ mm.

the lift force ($\propto 1/\tan\alpha$) that is required to have a droplet splash on a sphere at the same threshold as on a flat substrate (i.e. 0.12). Whilst the derivation (and values of m and s) was based upon spheres, Eqn. (1) predicts that $\alpha^* < \pi/3$ for convex surfaces ($r_s < 0$): $\beta(\alpha^*)$ increases in this case to account for the reduced splashing threshold identified in Section 3.1. The correction proposed therefore accounts for the effects of both positive and negative substrate curvature, as confirmed in Fig. 6.

In Eqn. (1), only the wedge angle has been modified in order to accommodate substrate curvature, whilst $\beta(\alpha)$ (with a fixed wedge angle) can successfully parameterise splashing thresholds of a wide range of low-viscosity fluids on flat substrates [10,41,40]. We thus expect that the wedge angle should not be affected by fluid properties on curved substrates either. Hence, the (geometrically-derived) effective wedge angle approach may be used to parameterise splashing thresholds on curved substrates for a wider range of low-viscosity fluids than studied here. Moreover, there is no strong dependence of substrate curvature on spreading rates on time scales relevant to splashing (see §3 of the Supplementary Material). This observation indicates that $\beta(\alpha^*)$ and θ may parameterise splashing on curved substrates of different wettabilities, as $\beta(\alpha)$ and θ can for flat substrates [10].

3.3. Asymmetric impacts

The results above pertain to axisymmetric impact ($c \approx 0$); in this section, we assess the effect of initial asymmetry between the impacting droplet and curved substrate via a horizontal offset from the axis of symmetry. Fig. 7a depicts the impact position on all $r_s \geqslant 2.0$ mm substrates investigated, from the perspective of a top-down view, with radial positions normalised by r_c. Only those experiments within the $\beta(\alpha)$ splashing threshold region for each substrate ($\beta(\alpha) \in [\beta_l, \beta_h]$ – see Section 3.1 for equivalent definitions in K) are displayed; these data correspond to all $r_s > 0$ points in Fig. 3b, in addition to $c/r_c > 0.15$ experiments (delineated by the orange-dashed circle in Fig. 7a). A pessimistic indication of the maximum error in determining the impact position (based on the cameras' minimum effective resolution) is indicated by the purple circle surrounding one point. Since only experiments within the splashing threshold regions (commensurate to the experimental error) are plotted, if asymmetry did not play a role in splashing outcomes here, then a uniform distribution would be expected in Fig. 7a. Such a distribution is seen for almost-axisymmetric impacts, but the splashing outcome is seen to dominate for experiments with $c/r_c \gtrsim 0.12$. Note that no such radial dependence would be expected if *all* experiments (i.e. both inside and outside the splashing threshold regions) were plotted. In summary, Fig. 7a suggests that modest offsets increase the splashing propensity of droplets close to the splashing threshold. To ensure that all axisymmetric impacts are included in the regime maps (Figs. 3 and 6), only $c/r_c < 0.15$ experiments are displayed.

Examples of typical non-axisymmetric impacts above the threshold region are shown in Figs. 7b and 7c. The whole offset is seen in the upper rows (from the perspective of one camera), whilst the offset is negligible ($< 0.01 r_c$) in the perpendicular direction (bottom rows, from the perspective of the other camera). Interestingly, non-axisymmetric splashing dynamics are seen in the negligible offset rows. We suggest that this observation results from inherently-3D effects influencing rim breakup due to a perturbation from the offset, which is best perceived from a bottom-up view of non-axisymmetric impact onto one of the concave surfaces, as shown in Fig. 7d ($c/r_c \approx 0.3$). Here, the gas beneath the lamella is harder to drain in the direction of the offset (with respect to the substrate apex, identified by a red circle), due to the upward-

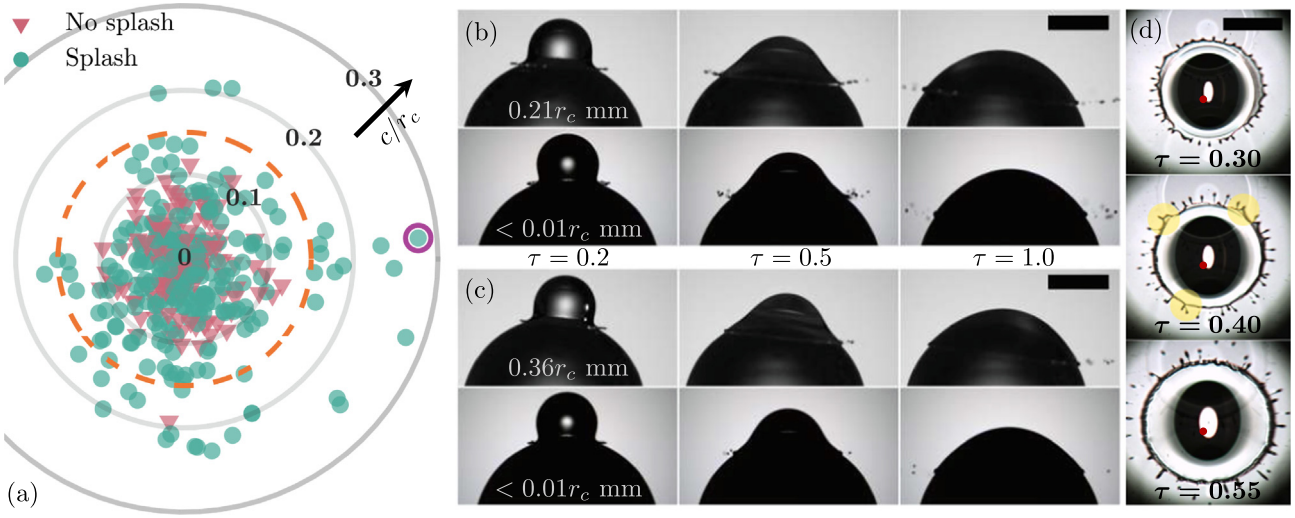

Fig. 7. Effect of asymmetry. (a) Impact position (centre axisymmetric) of every $r_s > 0$ experiment within the $\beta(\alpha)$ splashing threshold regions (all opaque $r_s > 0$ points in Fig. 3b; additional experiments with a larger offset), coloured by splashing outcome. The purple circle indicates the maximum error in impact position, based upon the minimum effective resolution of 34 pixels mm^{-1}. Only experiments within the orange dashed circle (indicating $c/r_c = 0.15$) are shown in the regime maps above. (b) We $= 482$; $\beta(\alpha) = 0.144$ impact onto a $r_s = 3.0$ mm sphere. Dimensional offsets in the *perpendicular* planes of view are indicated in each $\tau = 0.2$ frames. (c) Similar We $= 436$; $\beta(\alpha) = 0.141$ impact to panel (b), but with a larger offset. (d) Asymmetric We $= 345/\beta(\alpha) = 0.128$ impact (offset $c/r_c \approx 0.3$) onto a $r_s = -12.92$ mm substrate. Red points locate the substrate apex (approximately); yellow highlights indicate inherently 3D rim phenomena. All scale bars are 2 mm.

sloping substrate, so the lamella remains raised for longer in such directions. These asymmetric rim dynamics lead to the large distribution in satellite sizes and trajectories for a given impact, including due to the aforementioned 3D effects such as a splitting and merging of fingers (highlighted yellow in Fig. 7d). Also seen with non-zero offsets is film breakup in the body of the lamella, which can lead to long ligaments with substantial angular velocity that result in non-radial satellite trajectories. Note that many satellites land within the maximum spread length of the droplet in the direction of offset on concave surfaces, as the substrate curves substantially upwards to meet the satellites' trajectories. These 3D effects may play a role in the increase in splashing propensity seen with modest offsets for experiments close to the splashing threshold (identified in the previous paragraph), including the relatively-sharp radial transition seen in Fig. 7a.

In the offset views (top rows) of Figs. 7b and 7c, splashing is generally more pronounced in the 'downward' direction (towards the right here). Splashing can be suppressed in the 'upward' direction for larger offsets, as exhibited in Fig. 7c. These observations are consistent with known splashing behaviour on inclined flat substrates, where upward splashing is suppressed above a given substrate inclination, followed by the suppression of downward splashing at a yet greater inclination [47,48]. Under the theoretical framework from which $\beta(\alpha)$ is derived, the modification of splashing on inclined flat substrates stems from an effective reduction in impact velocity perpendicular to the substrate according to $\cos\eta$, where η is the substrate inclination. The lamella tip velocities therefore decrease with increasing η too, as does the lift force acting on the lamella itself, which in turn affects splashing. For a spherical substrate, η is the polar angle to the impact point from the vertical (similar to ϕ in Fig. 1e). Fig. 7c indicates that the mechanism of splashing modification on inclined flat substrates translates to curved substrates, so complete splashing suppression on spheres might be expected for even larger offsets than shown in Fig. 7c, though this is beyond the scope of our work.

Finally, it is interesting to note the relation of offsets from axisymmetry to the mechanism discussed in Section 3.2. Offsets decrease the effective substrate curvature in the upward direction, reducing the ability to drain gas from beneath the lamella, as elucidated in Section 3.2; conversely, the gas is easier to drain in the downward direction. Moreover, the substrate drops away from the lamella at a faster rate than in the downward direction compared to the upward direction, opening the effective wedge angle and reducing the splashing ratio. However, suppressed splashing is seen in the upward direction in Fig. 7c, which suggests that for large offsets the mechanism noted above for splashing suppression on tilted flat substrates may carry-over to curved substrates and the reduction in lamella tip velocities may be more significant than curvature-related effects.

4. Conclusions

This study has conclusively demonstrated that droplet splashing is significantly affected by the target substrate's curvature. Notably, we found that the radius of curvature, r_s plays a key role in the micromechanics of splashing. For axisymmetric impacts, splashing propensity was found to decrease monotonically with increasing $1/r_s$ over the uniquely-wide range of target geometries studied, including both convex ($r_s > 0$) and concave ($r_s < 0$) substrates, with a boundary value consistent with the known splashing behaviour on flat substrates ($r_s \to \infty$). Therefore, the splashing threshold is higher for smaller spheres compared to a flat substrate, whilst it is lower for concave surfaces. This new result for completely-dry surfaces diverges from related studies that considered wetted or continuously impinged spheres [25,26,28], in which splashing thresholds only appeared to change for the smaller spheres studied. We hypothesised that the alteration to the splashing thresholds seen in this work owes to a curvature-induced modification to the lift force acting on the advancing lamella at the point of breakup. Hence, we successfully incorporated the effect of substrate curvature into state-of-the-art splashing theory for flat substrates [5,29,40,41] via the introduction of an effective wedge angle between the lamella and substrate. Effects of asymmetry are only apparent for lateral offsets from axisymmetry greater than approximately 0.12, normalised by the droplet's radius of curvature at the point of impact. Inherently-3D dynamics are prevalent for asymmetric impact with a small offset, whilst splashing can be suppressed, at least in some directions, for larger

offsets. The latter result has parallels with splashing on inclined flat substrates [47,48]. Our results enhance the fundamental understanding of splashing in general, which is relevant to surfaces of other properties and geometries than the curved substrates we studied, but also indicate the potential for engineering textured substrates to reduce the distribution and aerosolisation of potentially-hazardous fluids by modifying droplet splashing dynamics.

Declaration of Competing Interest

The authors declare that they have no known competing financial interests or personal relationships that could have appeared to influence the work reported in this paper.

Funding acknowledgement

This work was funded by a Royal Society University Research Fellowship (Grant No. URF\R\180016) & Enhancement Award (Grant No. RGF\EA\181002) and two NSF/CBET-EPSRC grants (Grant Nos. EP/S029966/1 and EP/W016036/1).

Appendix A. Supplementary material

Supplementary data associated with this article can be found, in the online version, at https://doi.org/10.1016/j.jcis.2022.01.136.

References

[1] A.M. Worthington, R.S. Cole, IV. Impact with a liquid surface studied by the aid of instantaneous photography. Paper II, Philos. Trans. R. Soc. London, Ser. A 194 (252–261) (1900) 175–199. doi:10.1098/rsta.1900.0016.
[2] A.L. Yarin, Drop impact dynamics: splashing, spreading, receding, bouncing, Annu. Rev. Fluid Mech. 38 (2006) 159–192, https://doi.org/10.1146/annurev.fluid.38.050304.092144.
[3] C. Josserand, S.T. Thoroddsen, Drop impact on a solid surface, Annu. Rev. Fluid Mech. 48 (2016) 365–391, https://doi.org/10.1146/annurev-fluid-122414-034401.
[4] M.M. Driscoll, S.R. Nagel, Ultrafast interference imaging of air in splashing dynamics, Phys. Rev. Lett. 107 (15) (2011) 154502, https://doi.org/10.1103/PhysRevLett.107.154502.
[5] G. Riboux, J.M. Gordillo, Experiments of drops impacting a smooth solid surface: A model of the critical impact speed for drop splashing, Phys. Rev. Lett. 113 (2) (2014) 024507, https://doi.org/10.1103/PhysRevLett.113.024507.
[6] Y. Liu, P. Tan, L. Xu, Kelvin-Helmholtz instability in an ultrathin air film causes drop splashing on smooth surfaces, PNAS 112 (11) (2015) 3280–3284, https://doi.org/10.1073/pnas.1417718112.
[7] J. Palacios, J. Hernández, P. Gómez, C. Zanzi, J. López, Experimental study of splashing patterns and the splashing/deposition threshold in drop impacts onto dry smooth solid surfaces, Exp. Therm Fluid Sci. 44 (2013) 571–582, https://doi.org/10.1016/j.expthermflusci.2012.08.020.
[8] H. Almohammadi, A. Amirfazli, Droplet impact: Viscosity and wettability effects on splashing, J. Colloid Interface Sci. 553 (2019) 22–30, https://doi.org/10.1016/j.jcis.2019.05.101.
[9] H. Almohammadi, A. Amirfazli, Understanding the drop impact on moving hydrophilic and hydrophobic surfaces, Soft Matter 13 (10) (2017) 2040–2053, https://doi.org/10.1039/C6SM02514E.
[10] M.A. Quetzeri-Santiago, K. Yokoi, A.A. Castrejón-Pita, J.R. Castrejón-Pita, Role of the dynamic contact angle on splashing, Phys. Rev. Lett. 122 (22) (2019) 228001, https://doi.org/10.1103/PhysRevLett.122.228001.
[11] M.A.J. Van Limbeek, P.B.J. Hoefnagels, M. Shirota, C. Sun, D. Lohse, Boiling regimes of impacting drops on a heated substrate under reduced pressure, Phys. Rev. Fluids 3 (5) (2018) 053601, https://doi.org/10.1103/PhysRevFluids.3.053601.
[12] L. Bourouiba, The fluid dynamics of disease transmission, Annu. Rev. Fluid Mech. 53 (2021) 473–508, https://doi.org/10.1146/annurev-fluid-060220-113712.
[13] D. Khojasteh, N.M. Kazerooni, M. Marengo, A review of liquid droplet impacting onto solid spherical particles: A physical pathway to encapsulation mechanisms, J. Ind. Eng. Chem. 71 (2019) 50–64, https://doi.org/10.1016/j.jiec.2018.11.030.
[14] Y. Zhang, C. Tse, D. Rouholamin, P.J. Smith, Scaffolds for tissue engineering produced by inkjet printing, Cent. Eur. J. Eng. 2 (3) (2012) 325–335, https://doi.org/10.2478/s13531-012-0016-2.
[15] S.A. Banitabaei, A. Amirfazli, Droplet impact onto a solid sphere: Effect of wettability and impact velocity, Phys. Fluids 29 (6) (2017) 062111, https://doi.org/10.1063/1.4990088.
[16] G. Khurana, N. Sahoo, P. Dhar, Phenomenology of droplet collision hydrodynamics on wetting and non-wetting spheres, Phys. Fluids 31 (7) (2019) 072003, https://doi.org/10.1063/1.5103223.
[17] I. Yoon, S. Shin, Direct numerical simulation of droplet collision with stationary spherical particle: A comprehensive map of outcomes, Int. J. Multiphase Flow 135 (2021) 103503, https://doi.org/10.1016/j.ijmultiphaseflow.2020.103503.
[18] M.A. Quetzeri-Santiago, A.A. Castrejón-Pita, J.R. Castrejón-Pita, The effect of surface roughness on the contact line and splashing dynamics of impacting droplets, Sci. Rep. 9 (1) (2019) 1–10, https://doi.org/10.1038/s41598-019-51490-5.
[19] S. Bakshi, I.V. Roisman, C. Tropea, Investigations on the impact of a drop onto a small spherical target, Phys. Fluids 19 (3) (2007) 032102, https://doi.org/10.1063/1.2716065.
[20] A. Bordbar, A. Taassob, D. Khojasteh, M. Marengo, R. Kamali, Maximum spreading and rebound of a droplet impacting onto a spherical surface at low Weber numbers, Langmuir 34 (17) (2018) 5149–5158, https://doi.org/10.1021/acs.langmuir.8b00625.
[21] D. Khojasteh, A. Bordbar, R. Kamali, M. Marengo, Curvature effect on droplet impacting onto hydrophobic and superhydrophobic spheres, Int. J. Comput. Fluid Dyn. 31 (6–8) (2017) 310–323, https://doi.org/10.1080/10618562.2017.1349312.
[22] X. Liu, X. Zhang, J. Min, Maximum spreading of droplets impacting spherical surfaces, Phys. Fluids 31 (9) (2019) 092102, https://doi.org/10.1063/1.5117278.
[23] S. Chen, V. Bertola, Drop impact on spherical soft surfaces, Phys. Fluids 29 (8) (2017) 082106, https://doi.org/10.1063/1.4996587.
[24] S. Mitra, T.B.T. Nguyen, E. Doroodchi, V. Pareek, J.B. Joshi, G.M. Evans, On wetting characteristics of droplet on a spherical particle in film boiling regime, Chem. Eng. Sci. 149 (2016) 181–203, https://doi.org/10.1016/j.ces.2016.04.003.
[25] Y. Hardalupas, A. Taylor, J. Wilkins, Experimental investigation of sub-millimetre droplet impingement on to spherical surfaces, Int. J. Heat Fluid Flow 20 (5) (1999) 477–485, https://doi.org/10.1016/S0142-727X(99)00045-4.
[26] G. Charalampous, Y. Hardalupas, Collisions of droplets on spherical particles, Phys. Fluids 29 (10) (2017) 103305, https://doi.org/10.1063/1.5005124.
[27] G. Liang, Y. Guo, Y. Yang, S. Guo, S. Shen, Special phenomena from a single liquid drop impact on wetted cylindrical surfaces, Exp. Therm Fluid Sci. 51 (2013) 18–27, https://doi.org/10.1016/j.expthermflusci.2013.06.012.
[28] G. Liang, Y. Guo, X. Mu, S. Shen, Experimental investigation of a drop impacting on wetted spheres, Exp. Therm. Fluid Sci. 55 (2014) 150–157, https://doi.org/10.1016/j.expthermflusci.2013.06.012.
[29] J.M. Gordillo, G. Riboux, A note on the aerodynamic splashing of droplets, J. Fluid Mech. 871 (2019) R3, https://doi.org/10.1017/jfm.2019.396.
[30] T.C. Sykes, Internal dynamics of coalescing droplets Ph.D. thesis, University of Leeds, 2020.
[31] M.A. Quetzeri-Santiago, J.R. Castrejón-Pita, A.A. Castrejón-Pita, On the analysis of the contact angle for impacting droplets using a polynomial fitting approach, Exp. Fluids 61 (2020) 1–13, https://doi.org/10.1007/s00348-020-02971-1.
[32] E. Li, M.-J. Thoraval, J. Marston, S.T. Thoroddsen, Early azimuthal instability during drop impact, J. Fluid Mech. 848 (2018) 821–835, https://doi.org/10.1017/jfm.2018.383.
[33] Q. Liu, J.H.Y. Lo, Y. Li, Y. Liu, J. Zhao, L. Xu, The role of drop shape in impact and splash, Nat. Commun. 12 (1) (2021) 1–8, https://doi.org/10.1038/s41467-021-23138-4.
[34] C. Lin, K. Zhang, X. Chen, L. Xiao, S. Chen, J. Zhu, T. Zou, Reducing droplet contact time and area by craterlike surface structure, Phys. Rev. Fluids 6 (8) (2021) 083602, https://doi.org/10.1103/PhysRevFluids.6.083602.
[35] Y. Wang, L. Bourouiba, Unsteady sheet fragmentation: droplet sizes and speeds, J. Fluid Mech. 848 (2018) 946–967, https://doi.org/10.1017/jfm.2018.359.
[36] H. Zhang, Y. Gao, X. Zhang, X. Yi, Y. Du, F. He, Z. Jin, P. Hao, Characteristics of secondary droplets produced by the impact of drops onto a smooth surface, Adv. Aerodyn. 3 (1) (2021) 1–12, https://doi.org/10.1186/s42774-021-00091-w.
[37] J.C. Bird, S.S.H. Tsai, H.A. Stone, Inclined to splash: triggering and inhibiting a splash with tangential velocity, New J. Phys. 11 (6) (2009) 063017, https://doi.org/10.1088/1367-2630/11/6/063017.
[38] R.L. Vander Wal, G.M. Berger, S.D. Mozes, The combined influence of a rough surface and thin fluid film upon the splashing threshold and splash dynamics of a droplet impacting onto them, Exp. Fluids 40 (1) (2006) 23–32. doi:10.1007/s00348-005-0043-3.
[39] L. Xu, W.W. Zhang, S.R. Nagel, Drop splashing on a dry smooth surface, Phys. Rev. Lett. 94 (18) (2005) 184505, https://doi.org/10.1103/PhysRevLett.94.184505.
[40] G. Riboux, J.M. Gordillo, Boundary-layer effects in droplet splashing, Phys. Rev. E 96 (1) (2017) 013105, https://doi.org/10.1103/PhysRevE.96.013105.

[41] T.C. de Goede, N. Laan, K.G. De Bruin, D. Bonn, Effect of wetting on drop splashing of newtonian fluids and blood, Langmuir 34 (18) (2018) 5163–5168, https://doi.org/10.1021/acs.langmuir.7b03355.
[42] P. García-Geijo, E.S. Quintero, G. Riboux, J.M. Gordillo, Spreading and splashing of drops impacting rough substrates, J. Fluid Mech. 917 (2021) A50, https://doi.org/10.1017/jfm.2021.313.
[43] M. Usawa, Y. Fujita, Y. Tagawa, G. Riboux, J.M. Gordillo, Large impact velocities suppress the splashing of micron-sized droplets, Phys. Rev. Fluids 6 (2) (2021) 023605, https://doi.org/10.1103/PhysRevFluids.6.023605.
[44] C.A. Papakonstantinou, H. Chen, A. Amirfazli, New ellipse fitting method for contact angle measurement, Surf. Innovations (2021) 1–9, https://doi.org/10.1680/jsuin.21.00028.
[45] J.F. Joanny, P.-G. De Gennes, A model for contact angle hysteresis, J. Chem. Phys. 81 (1) (1984) 552–562, https://doi.org/10.1063/1.447337.
[46] D. Bonn, J. Eggers, J. Indekeu, J. Meunier, E. Rolley, Wetting and spreading, Rev. Mod. Phys. 81 (2) (2009) 739, https://doi.org/10.1103/RevModPhys.81.739.
[47] Š. Šikalo, C. Tropea, E. Ganić, Impact of droplets onto inclined surfaces, J. Colloid Interface Sci. 286 (2) (2005) 661–669, https://doi.org/10.1016/j.jcis.2005.01.050.
[48] J. Hao, J. Lu, L. Lee, Z. Wu, G. Hu, J.M. Floryan, Droplet splashing on an inclined surface, Phys. Rev. Lett. 122 (5) (2019) 054501, https://doi.org/10.1103/PhysRevLett.122.054501.